Effect of ambient conditions on performance and current distribution of a polymer electrolyte membrane fuel cell

T. HOTTINEN*, M. NOPONEN, T. MENNOLA, O. HIMANEN, M. MIKKOLA and P. LUND
Helsinki University of Technology, Laboratory of Advanced Energy Systems, PO Box 2200, Fin-02015 HUT, Finland
(*author for correspondence, fax: +358 9 451 3195, e-mail: tero.hottinen@hut.fi)

Abstract

The performance and current distribution of a free-breathing polymer electrolyte membrane fuel cell (PEMFC) was studied experimentally in a climate chamber, in which temperature and relative humidity were controlled. The performance was studied by simulating ambient conditions in the temperature range 10 to 40 °C. The current distribution was measured with a segmented current collector. The results indicated that the operating conditions have a significant effect on the performance of the fuel cell. It was observed that a temperature gradient between the fuel cell and air is needed to achieve efficient oxygen transport to the electrode. Furthermore, varying the air humidity resulted in major changes in the mass diffusion overpotential at higher temperatures.

1. Introduction

Although the main part of PEMFC research efforts is focused on transportation and kW-scale stationary power applications, small and portable fuel cells may also have strong market potential. Small PEMFCs are considered as a replacement for batteries in a wide range of portable electronic devices [1–3].

In a small PEMFC system, the simplicity and power density of the system are usually crucial design criteria. For example, the use of free convection for oxygen transport to the cathode may be desirable to eliminate power-consuming fans and compressors. Hence, it is necessary to be able to compare the power losses caused by the use of free convection to the use of forced oxygen feed. However, the existing literature on free convection fuel cells is inadequate to make these conclusions and thus more experimental and theoretical work is needed.

The free convective force in a fuel cell is caused by density gradients in the air. These arise from temperature differences inside the cell, temperature differences between the cell and ambient air, and decreasing partial pressure of oxygen and increasing partial pressure of water vapour inside the cell. The power density of the cell influences the above mentioned factors; the temperature gradients are formed because of the entropy produced and partial pressure gradients by the fuel cell reactions, and the ambient conditions define the magnitude of these gradients.

In this study the performance of a free-breathing PEMFC was studied in a climate chamber in which the temperature and humidity of air were varied. The effect of varying ambient conditions on the current distribution, and thus also power distribution, of the cell was studied with a segmented flow-field plate.

2. Experimental details

The measurements were performed with a unit fuel cell having an active area of 5 cm × 5 cm placed inside a climate chamber. The fuel cell components used in the measurements are listed in Table 1. The cathode side flow-field plate was segmented into 48 electrically isolated fragments in order to measure the current distribution of the fuel cell. The measurement system has been presented previously in [4, 5]. Each segmented current collector pin was connected through a 0.1 Ω high-precision resistor (accuracy ±5 mΩ) to a Globe-Tech, Inc. load unit. The voltage drop $u_{i,j}$ over each resistor was monitored with a Hewlett Packard 75000 Series B data logger. The current densities $i_{i,j}$ were then calculated from Ohm's law:

$$i_{i,j} = \frac{u_{i,j}}{RA/n} = \frac{19.2 * u_{i,j}/\Omega}{\Omega \times u_{i,j}} \qquad (1)$$

where i, j refer to a certain segment, R to the resistance of one resistor (0.1 Ω), A to the active area of the cell (25 cm^2), and n to the total number of current collector pins (48). The error resulting from this simplified formula is discussed in [4, 5]. In this study we had to use longer current cables to be able to use the measurement system in the climate chamber. The total resistance

Table 1. Fuel cell components used in the measurements

Component	Description	Manufacturer
Combined anode side end plate/current collector	1 cm thick gold plated copper plate	GlobeTech, Inc. modified by authors
Anode side flow-field plate	Machined graphite plate for 25 cm^2 fuel cell, column flow pattern	GlobeTech, Inc.
Gas diffusion backings	Carbon paper, Sigracet® GDL10-BB	SGL Technologies GmbH/SGL Carbon Group
MEA	Primea® MEA Series 5510 Cleo	W.L. Gore & Associates
Combined cathode side flow-field plate/ current collector/end plate	Straight open-to-air channel pattern [4]	Authors

of the 0.1 Ω resistors and current cables between each segment and the load was 0.3 Ω ± 0.03 Ω. This increases the polarization between different cell segments and thus the current distributions calculated by Equation 1 are somewhat smoother than the real distributions [4].

The GlobeTech, Inc. gas handling unit was used to control the hydrogen mass flow. In the measurements, the minimum flow of hydrogen was set to 26 cm^3 min^{-1} and for larger flows a current-based relation of 10 cm^3 A^{-1} min^{-1} was used (a stoichiometry of 1.5). The flow rate was controlled with a MKS type 1179A Mass-Flo® Controller having the accuracy of ±5 cm^3 min^{-1} in the range of 10–500 cm^3 min^{-1}. Hydrogen having purity of 99.999% was fed into the cell at atmospheric pressure and without humidification from a pressure bottle. Since the fuel cell used was of free-breathing type, the oxygen was taken directly from the air inside the climate chamber. The built-in current interrupter circuitry in the GlobeTech, Inc. load unit used to monitor the cell resistance could not be used, because the lengthened current cables caused additional impedance. This interfered the measurement of the voltage transient used in the determination of resistance.

The fuel cell was placed in a metal box to prevent the airflow caused by the fan of the climate chamber control system from affecting the cell performance. The metal box had holes in its bottom and cover to enable ambient conditions inside the box to be equal with the rest of the climate chamber. The effect of the climate chamber control system on the fuel cell performance was evaluated before the measurement series. This was done by measuring polarization curves in similar conditions when the climate chamber fan was on and off. The temperature and relative humidity in these measurements were 30.6 °C and 38.5%. The comparison of these polarization curves, illustrated in Figure 1, show that the chamber had virtually no effect on the performance of the cell.

The conditions of the climate chamber could be controlled by two different methods. In direct temperature control, an electric resistor and a cooling compressor control the temperature of the chamber. The relative humidity of the chamber could not be directly controlled in this mode and it is dependent on the conditions of air outside the chamber. In indirect temperature control, temperature and humidity are simultaneously controlled with a heat exchanger and
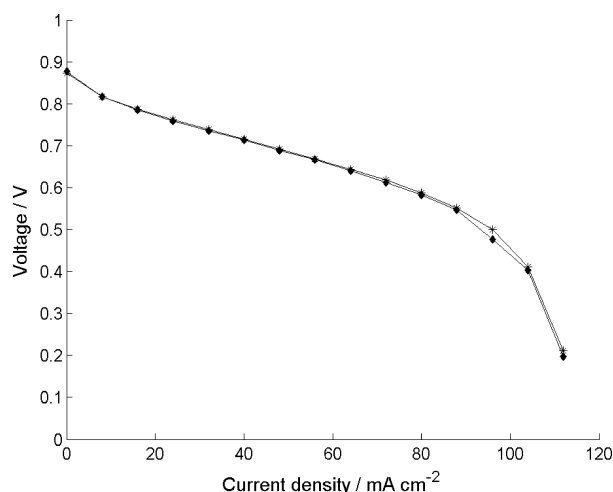

Fig. 1. Effect of the climate chamber control system on the performance of the fuel cell. Key: (✳) Chamber off; (♦) Chamber on.

by heating or cooling a water basin inside the chamber. The lowest achievable condensation point in indirect temperature control was 12 °C. This sets limit to the lowest achievable stable relative humidity in different temperatures. In conditions where non-direct temperature control could not be used, the humidity was controlled by adding water basins in the chamber outside the metal box.

Three PCs were used to control the measurement equipment and to collect the measurement data. A schematic of the whole measurement system used is illustrated in Figure 2.

The performance of the fuel cell was analysed by simultaneously measuring the polarization curve and current distribution of the cell. The polarization curves were measured in a current scan mode with steps of 0.2 A (8 mA cm^{-2}) and the voltage was allowed to stabilize for 30 s at each point before increasing the current. Before the polarization curve measurements, the climate chamber was allowed to stabilize for an hour and after that the fuel cell was allowed to stabilize for an additional 15 min at a current density of 100 mA cm^{-2} in order to achieve reproducible conditions for each measurement. The cathode was dried between the measurements with a strong air pulse from a compressed-air hose to remove liquid water.

The measurement system measured the current distribution approximately once every two seconds. The
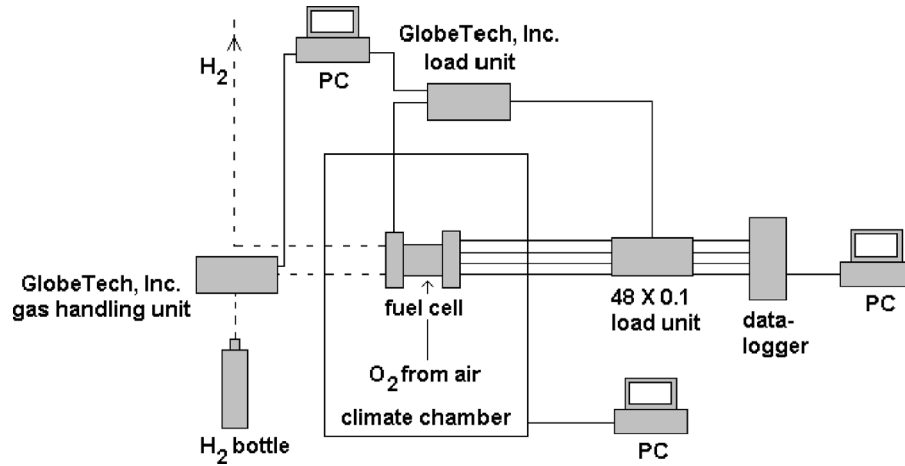
Fig. 2. Schematic of measurement system.

current density data for each pin was averaged over the measured data for each current level. The first and last current density readings from each current level were ignored in order to eliminate the effect of possible transitions occurring during the current density measurement.

The ambient temperatures (T_{amb}) and relative humidity (ϕ) used in the measurement series are listed in Table 2. The conditions where direct temperature control was used are denoted with an asterisk. The variation in temperature and relative humidity of the climate chamber during the measurements were ±0.1 °C and ±0.5%, and they were measured with a Vaisala HMP233 sensor (accuracy ±0.1 °C and ±1%). The absolute humidity (x) at different conditions are also listed in Table 2. These were calculated as

$$x = \frac{M_v p_v}{M_a p_a} = 0.6220 \left(\frac{p_v}{p_{amb} - p_v} \right) \tag{2}$$

where M is the molar mass, p the partial pressure, and p_{amb} atmospheric pressure (∼1.013 bar). Subscripts 'v' and 'a' refer to water vapour and air, respectively. The partial pressure of water vapour is calculated as

$$p_v = \phi p'_v \tag{3}$$

where ϕ is the relative humidity and p'_v is the partial pressure of saturated water vapour. The partial pressures of saturated water vapour at different temperatures are well tabulated in the literature (e.g., [6]).

The cell temperature (T_{cell}) was not controlled during the measurements but it was measured with a temperature probe located in a hole drilled into the anode side flow-field plate. The cell temperatures remained quite constant during the polarization measurements and are listed in Table 2. The accuracy of the temperature probe was ±1 °C.

Table 2. Ambient temperatures (T_{amb}) and relative humidity (ϕ) levels used in the measurements, with corresponding absolute humidity (x) and cell temperatures (T_{cell})

T_{amb} /°C	ϕ /%	x	T_{cell} /°C
10	25.5*	0.0019	21–22
	41.5*	0.0031	20–21
	59*	0.0045	21
20	32*	0.0046	27–28
	46*	0.0067	26
	60	0.0087	26
	75	0.011	27
	90	0.013	27
30	45	0.012	32–33
	60	0.016	33–34
	75	0.020	33
	90	0.024	33
40	24.5	0.011	44
	45	0.021	43–44
	60	0.028	43
	75	0.036	43–44
	90	0.044	44

Conditions where direct temperature control was used are denoted with an asterisk.

3. Results

The polarization curves from the measurements are illustrated in Figure 3. The legends in Figure 3 refer to the relative humidity of the corresponding measurement. It was noticed that the ambient temperature has a significant effect on the performance of the cell. Maximum current densities could be achieved with the lowest ambient temperatures because the temperature gradient between the cell and ambient air was at its maximum (Table 2). Because buoyancy force is directly proportional to the temperature gradient, the air velocity in the gas channel should have also been at its maximum with the lowest ambient temperature. This implies that the partial pressure of oxygen was most uniform with the lowest ambient temperatures and thus the cell performance was better.
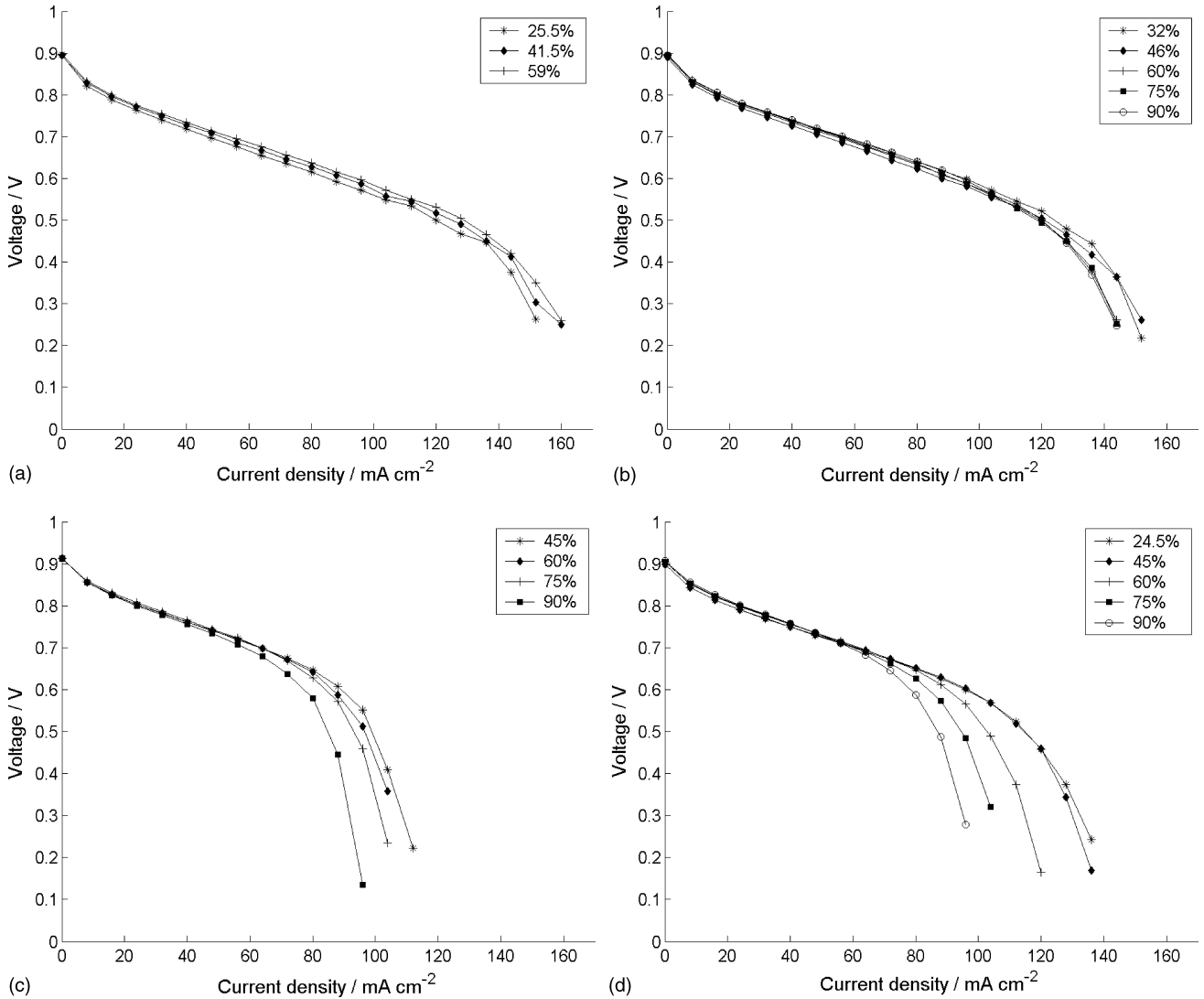
Fig. 3. Polarization curves from measurements at T_{amb}: (a) 10, (b) 20, (c) 30 and (d) 40 °C.

When the ambient temperature was increased, the temperature gradient was simultaneously decreased because the cell was not thermally insulated and the cell might not have reached its equilibrium temperature. The increased ambient temperature together with increased absolute humidity decreased the performance of the cell. This implies that the airflow velocity was not strong enough to remove adequately the excess water from the cathode, resulting in flooding of the gas diffusion backing and electrode.

Although we could not measure the cell resistance, the data from the polarization curves implies that the differences in the cell performance could not be explained with changed resistances of the proton conductive phases. This conclusion can be made by comparing the ohmic parts (i.e., the linear parts) of the different polarization curves, which are all almost identical. Moreover, the comparison of the polarization curves reveals that the ambient conditions had a minor effect on the activation overpotential.

Although some information can be obtained from the normal polarization curves, they do not give informa-

tion on the current distribution in the cell. The current distribution reflects the partial pressure distribution of oxygen at the fuel cell electrode and thus gives more detailed information on cell conditions.

In the current distribution figures, the vertical and horizontal axes refer to the orientation of the cathode flow channels. The bar (1,1) is the left upper part and (4,12) the right lower part of the cell. The matrix notation (i, j) refers to a segment that is located in vertical position i and horizontal position j. The airflow in Figures 4 and 5 is in direction of $(4, j) \rightarrow (1, j)$. The pins (3, 2) and (4, 5) had poor electrical contact and thus there is a pronounced drop on the current distributions at these points. The poor electrical contact of these pins also exaggerates the current density achieved from the adjacent pins. However, small differences in the contact resistances of the segments do not affect the electrode kinetics significantly [5].

Dry hydrogen was fed into the cell from the right lower part. This explains the pronounced drop in the current densities of pin (4,12), because the hydrogen had a drying effect on the proton conducting phases of that
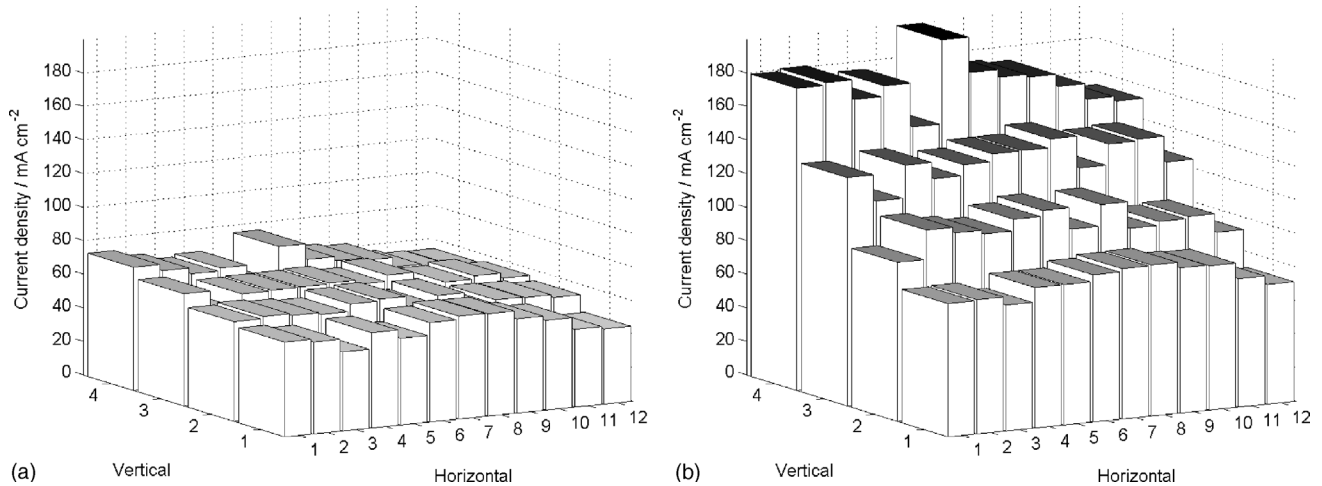
Fig. 4. Current distributions from measurement $T_{amb} = 20\ °C$ and $\phi = 46\%$. Average current density (a) 56 mA cm^{-2}; (b) 120 mA cm^{-2}.

area resulting in lower conductivity. Similar behavior was observed in previous measurements [4, 5].

The current distributions were quite even in the regions where the mass diffusion overpotential was not dominant, that is, at current densities where a down slope of the polarization curve does not occur. In regions where the mass diffusion overpotential is significant, the current distributions became more uneven. In these regions, most of the current was produced in the lower parts of the fuel cell. This implies that at higher current densities free convection was not strong enough to transfer equal amount of oxygen along the electrode. Examples of even and uneven current distributions are illustrated in Figure 4.

Figure 5 illustrates the current distributions at an ambient temperature of 40 °C while varying the relative humidity. The average current density is 96 mA cm^{-2} in all figures. The current distribution is more uniform at low humidity levels and becomes more uneven with increased humidity. Because the temperature gradient between the cell and ambient air did not depend on the humidity level (Table 2), the airflow velocities were approximately the same in all cases. Furthermore, the partial pressure of oxygen is not strongly dependent on the humidity at 40 °C; the difference in oxygen partial pressure between dry and fully saturated air is only about 5%. The current distribution is therefore caused by flooding, which prevents oxygen reaching the electrode. It is also clear from Figure 5 that the flooding starts from the upper parts of the cell and, with increased humidity, flooding spreads downwards and blocks more of the electrode.

It is obvious that possible flooding starts from the end of the channels, because the air flow transports product water with it, and thus there will be more water vapour or even liquid water at the ends of the channels. This phenomenon can also be seen in the results of two-phase modelling studies on forced convection fuel cells, for example, by You and Liu [7] and Wang et al. [8]. Moreover, it was observed that the possible condensation of water occurs in the top parts of the cell in a

single-phase modelling study by Mennola et al. [9]. The simulated cell geometry in [9] was the same as in this study.

4. Conclusions

The performance of a free-breathing PEMFC was studied by simulating a wide range of ambient conditions in a climate chamber and measuring its current distribution and polarization curves. The results showed that the ambient conditions have a significant effect on the cell performance.

The cell performance was best at low ambient temperatures, because the temperature gradient between the cell and air was at its maximum. Thus, the airflow velocity was also at its maximum, leading to more effective oxygen transport and water removal. The cell performance decreased with increased ambient temperature because the temperature gradient between the cell and air decreased, resulting in decreased airflow velocity and, thus, in increased mass transfer limitations in the cathode. At higher temperatures and high humidity, the airflow rate was not strong enough to remove water from the cathode and flooding was observed. The results also indicated that absolute temperature had a minor effect on cell performance, because the mass transfer limitations were already significant at fairly low current densities.

Current distribution measurements also showed that the flooding starts from the top section of the cell, that is, from the end of the gas channels. This phenomenon can also be concluded from the modelling studies with free and forced convection [7–9].

To design a fuel cell that performs well even in harsh ambient conditions, adequate airflow must be provided to the cathode to ensure uniform oxygen concentration distribution and effective water removal. If forced convection is used, the fuel cell performance is usually better than with free convection. However, the additional fan or compressor increases the complexity
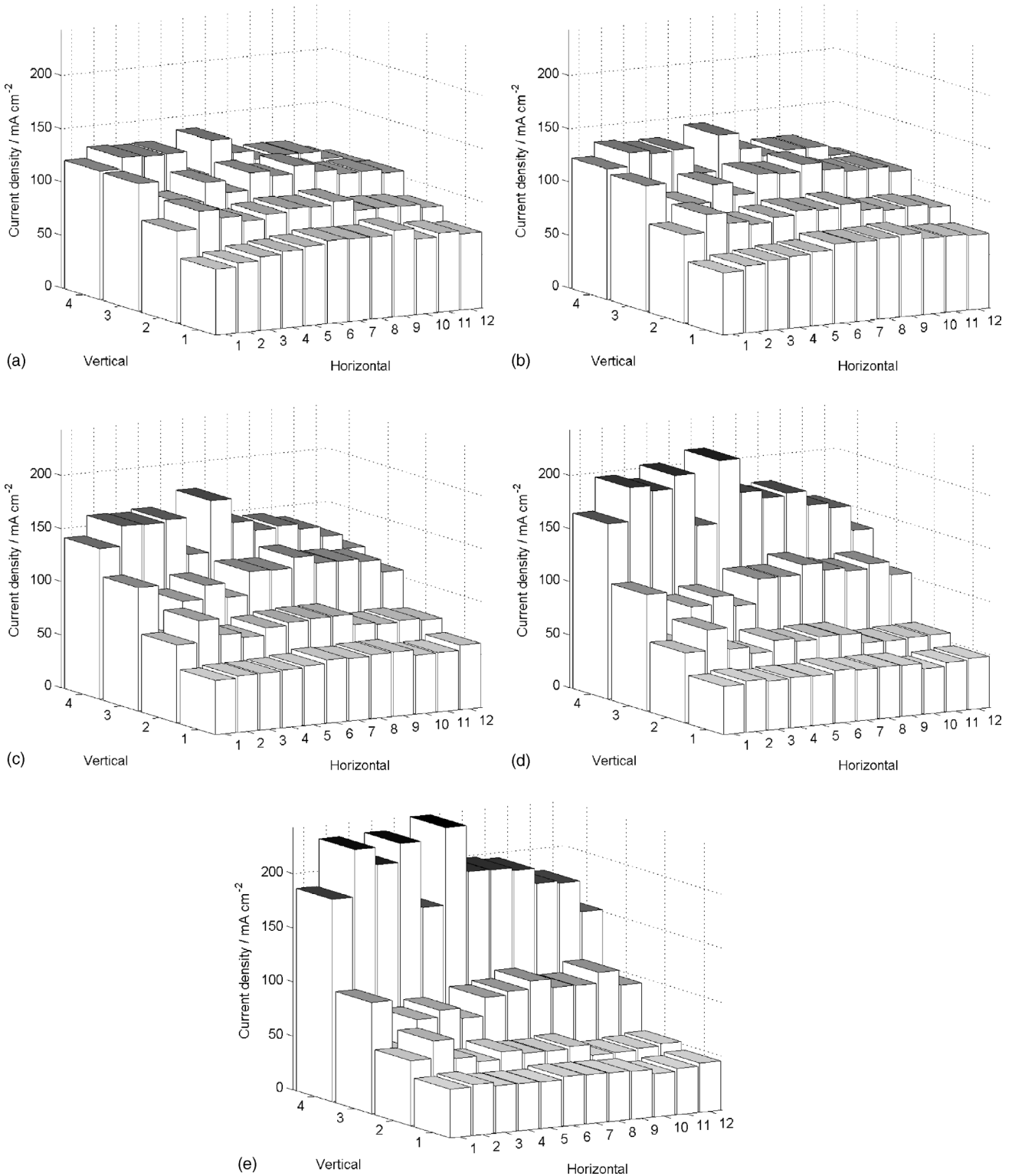
Fig. 5. Current distributions at average current density 96 mA cm^{-2} from measurements at $T_{amb} = 40$ °C and different relative humidities, ϕ. ϕ: (a) 24.5%, (b) 45%, (c) 60%, (d) 75% and (e) 90%.

of the system, and thus may decrease the energy density of the fuel cell system. However, if free convection is preferred the cell design has to be further developed. This includes optimization of flow geometries and cell materials, which may both differ radically from the optimized forced convection fuel cell. Examples of geometric designs for free-breathing cells are the

pseudo-bipolar and strip designs [10, 11], and examples of novel material solutions are metal foams [12] and sinter structures [13]. The optimized material for free breathing fuel cells should have low thermal conductivity, so that temperature gradients are pronounced between the cell and the ambient air. However, if the thermal conductivity is too low, the fuel cell warms

up, which might be undesirable in portable applications.

Acknowledgements

References

1. C.K. Dyer, *J. Power Sources* **106** (2002) 31.
2. J.P. Meyers and H.L. Maynard, *J. Power Sources* **109** (2002) 76.
3. T.B. Atwater, P.J. Cygan and C.L. Fee, *J. Power Sources* **91** (2000) 27.
4. M. Noponen, T. Mennola, M. Mikkola, T. Hottinen and P. Lund, *J. Power Sources* **106** (2002) 304.
5. M. Noponen, T. Hottinen, T. Mennola, M. Mikkola and P. Lund, *J. Appl. Electrochem.* **32** (2002) 1081.
6. D.R. Lide (Ed.), 'CRC Handbook of Chemistry and Physics', 78th edn (CRC Press, Bocca Raton, 1997).
7. L. You and H. Liu, *Int. J. Heat Mass Transf.* **45** (2002) 2277.
8. Z.H. Wang, C.Y. Wang and K.S. Chen, *J. Power Sources* **94** (2001) 40.
9. T. Mennola, M. Noponen, M. Aronniemi, T. Hottinen, M. Mikkola, O. Himanen and P. Lund, *J. Appl. Electrochem.*, submitted.
10. R. Jiang and D. Chu, *J. Power Sources* **93** (2001) 25.
11. H. Chang, J.R. Kim, J.H. Cho, H.K. Kim and K.H. Choi, *Solid State Ionics* **148** (2002) 601.
12. S. Le, R. Platon, Q. Fan and R. Kot, *Int. Patent WO 02 059 998* (2002).
13. P. Mitchell, *Int. Patent WO 9 852 241* (1998).